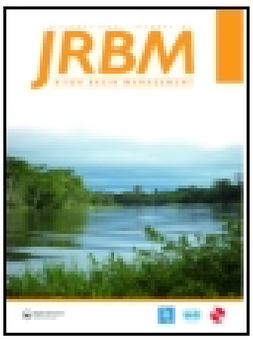

International Journal of River Basin Management

ISSN: 1571-5124 (Print) 1814-2060 (Online) Journal homepage: https://www.tandfonline.com/loi/trbm20

Practical modelling of tidal propagation under fluvial interaction in the mekong delta

Hiroshi Takagi, Nguyen Hong Quan, Le Tuan Anh, Nguyen Danh Thao, Van Pham Dang Tri & Tran The Anh

To cite this article: Hiroshi Takagi, Nguyen Hong Quan, Le Tuan Anh, Nguyen Danh Thao, Van Pham Dang Tri & Tran The Anh (2019): Practical modelling of tidal propagation under fluvial interaction in the mekong delta, International Journal of River Basin Management, DOI: 10.1080/15715124.2019.1576697

To link to this article: https://doi.org/10.1080/15715124.2019.1576697

Accepted author version posted online: 30 Jan 2019.

Submit your article to this journal

Article views: 2

View Crossmark data

Full Terms & Conditions of access and use can be found at
https://www.tandfonline.com/action/journalInformation?journalCode=trbm20

Publisher: Taylor & Francis & International Association for Hydro-Environment Engineering and Research
Journal: *Intl. J. River Basin Management*
DOI: 10.1080/15715124.2019.1576697

Check for updates

PRACTICAL MODELLING OF TIDAL PROPAGATION UNDER FLUVIAL INTERACTION IN THE MEKONG DELTA

HIROSHI TAKAGI
Tokyo Institute of Technology, School of Environment and Society, 2-12-1 Ookayama, Meguro-ku, Tokyo 152-8550, Japan, takagi@ide.titech.ac.jp
NGUYEN HONG QUAN
Vietnam National University - Ho Chi Minh city (VNU-HCM), Center of Water Management and Climate Change (WACC), A3 Street, Dong Hoa Ward, Di An Town, Binh Duong, Vietnam, hongquanmt@yahoo.com
LE TUAN ANH
Tokyo Institute of Technology, School of Environment and Society, 2-12-1 Ookayama, Meguro-ku, Tokyo 152-8550, Japan, letuananh.aa@m.titech.ac.jp
NGUYEN DANH THAO
Ho Chi Minh City University of Technology, Faculty of Civil Engineering, 268 Ly Thuong Kiet St., Dist. 10, Ho Chi Minh City, Vietnam, ndthao@hcmut.edu.vn
VAN PHAM DANG TRI
Can Tho University, College of Environment and Natural Resources, Campus II, 3/2 street, Ninh Kieu district, Can Tho City, Vietnam, vpdtri@ctu.edu.vn
TRAN THE ANH
Vietnam Institute of Seas and Islands, 125 Trung Kinh Street, Cau Giay district, Hanoi, Vietnam, trantheanhv9@gmail.com

ACCEPTED MANUSCRIPT

Abstract

Estuarine/river engineers often encounter a problem that it is hard to specify an upstream boundary of a delta in the numerical modelling because of lack of good quality discharge data. This paper proposes a practical procedure to simulate tidal propagation and damping over a river stretch using a commonly used shallow-water equation model without imposing an upstream discharge boundary. The interaction between tides and river flows could be easily evaluated by applying seasonally-varying Manning's *n* friction values. The Hau River, one of the main streams of the Mekong River, is studied by analysing water levels measured at three different locations in the estuary. The nearly straight-line geometry of the Hau River allows us to neglect flood plain sinuosity, making it possible to extract tidal damping induced purely by fluvial influence. A series of analyses, including spectrum analysis and hydrodynamic simulation, suggests that tidal damping in the estuary of the Mekong Delta can be readily reproduced using the numerical model with Manning's *n* values of 0.025–0.032 [s $m^{-1/3}$] for the flood season and 0.018–0.025 for the dry season. The present study demonstrates that changes in Manning's *n* value according to river flow conditions result in more reliable estimations than simply using a constant value throughout the year. The proposed procedure will be of great benefit not only for tidal modelling but also river and urban flood simulations, saline intrusion modelling and sea-level rise projections in the estuary of the Mekong River.

***Keywords*: Mekong Delta, Ocean tidal propagation, River discharge, Shallow-water equation, Manning's *n* value, practical simulation**

1. Introduction

Tidal damping is an important physical phenomenon to be considered in ocean tide modelling, particularly when tides propagate upstream in a low-lying estuary and interact with river discharge that flows in a counter direction. The degree of the damping is determined by the balance between energy loss and concentration when ocean tides propagate over a long distance in a delta (Godin, 1999; Savenije, 2001). In addition to bottom friction, river discharge and changing river geometry are also

ACCEPTED MANUSCRIPT

factors that damp tide amplitudes and decrease tide celerity (Vongvisessomjai and Srivihok, 2003). It is also noted that tides are not always damped, but sometimes tend to be amplified particularly when waves move faster than theoretical wave celerity. For example, tidal amplification was observed in the estuary of the Schelde and the St. Lawrence River (Savenije *et al*., 2008, Matte *et al*., 2017a). The degree of tidal damping can be estimated by an analytical expression for ideal estuaries. The nonlinearized St. Venant equations can be applied to an exponentially converging channel (Savenije, 2001; Savenije *et al*., 2008). Such analytical solutions are powerful for investigating the fundamental characteristics of tidal damping and amplification in estuarine environments. However, for engineering purposes, mathematical expressions are not always applicable, especially for a river that exhibits complex geometries such as a naturally meandering shape, straight concrete dykes, sandbanks or landfills in-stream, and many tributaries or canals connected to the main stream.

In the fields of coastal and ocean engineering, 2D shallow-water equation models are commonly used to simulate long-wave phenomena such as ocean tides, tsunamis, storm surges, and coastal floods because of their versatility and applicability to complex geometries and relatively small computational load (*e.g.*, Sasaki *et al*., 2012, Takagi and Bricker, 2014b; Tasnim *et al*., 2014; Takagi *et al*., 2016c). Nevertheless, it should be noted that the shallow-water models, which assumes depth-averaged velocities, do not precisely account for vertical mixing flows caused by oceanic and fluvial interactions. Thus, the mechanisms of turbulence in flows need to be investigated more precisely by using a 3D hydrodynamic model, such as those incorporating a turbulence and dissipation model based on Reynolds-averaged Navier-Stokes equations (RANS) or Large Eddy Simulation (LES). However, such sophisticated models appear to pose extensive computational costs to perform a simulation that encompasses a long stretch of the river (typically, a few hundreds of km) subjected to oceanic and fluvial interactions (Takagi *et al*., 2016d).

In the Mekong Delta, which extends over low-lying land, tidal damping is especially pronounced during the flood season (Takagi *et al*., 2015). The Mekong Delta is also vulnerable to the influence of sea-level rise (SLR) and land subsidence (Wassmann *et al*., 2004; Dasgupta *et al*., 2007; Dang *et al*., 2016; Nhan, 2016; Takagi *et al*., 2016a). At present, about 1.7 million ha of land are flooded every year, affecting

ACCEPTED MANUSCRIPT

9 million people not only in the vicinity of the coastline but also in inland regions (Thuy and Furukawa, 2007). Assuming an SLR scenario of 25 cm by 2050, based on the IPCC AR5's projections (IPCC, 2013), the duration of inundation in Can Tho City (the most populous city in the Mekong Delta at 1.2 million people) will increase from 2.5% of the year at present to 7.5% (Takagi *et al.*, 2014a). However, the projection becomes much more serious when accelerated relative SLR (RSLR) due to continuing land subsidence in the region is considered (Esteban *et al.*, 2019). If groundwater pumping continues at the present rates, ~0.88 m (0.35–1.4 m) of land subsidence is expected by 2050. As a result, the Mekong Delta will likely experience ~1 m (0.42–1.54 m) of additional inundation hazard (Erban *et al*., 2014). The duration of inundation of important roads in Can Tho will continue to rise from the current value of 72 inundated days per year to 270 days by 2030 and 365 days by 2050 because of the combined influence of SLR and land subsidence (Takagi *et al*., 2016a). Given the emerging threat of RSLR, more accurate prediction of ocean tidal propagation in the Mekong Delta is required because tides predominantly determine water elevation, even in upstream locations (Takagi *et al*., 2018, Chang *et al*., 2019). The semi-diurnal component can be considered a governing factor in water elevation, followed by the diurnal and annual components. Amongst all tidal components, the M2 semidiurnal tidal component appears to have the strongest influence (Takagi *et al*., 2016b). The maximum water levels in the Mekong Delta are considered to be rising faster than the global SLR, because tides, especially semi-diurnal components, are being amplified by SLR because of multiple reasons (e.g., the increasing celerity of tidal waves; Nhan, 2016). Hoang *et al*. (2016) performed the CMIP5 climate model and projected that both seasonal and annual river discharges in the Mekong's hydrological cycle will be increased by +5 to +16 % under future climate change. A combination of changes in upstream discharge, rainfall, and sea levels will also exacerbate salinity intrusion in the Mekong Delta (Tran Anh *et al*., 2018).

Given these backgrounds, estimating how tidal amplitudes are influenced by the interaction with river flows is very important in predicting water levels (WLs) along the Mekong River. However, engineers/scientists often encounter a problem that it is hard to specify an upstream boundary in the numerical modelling because of lack of

ACCEPTED MANUSCRIPT

discharge data or less reliable upstream boundary that is located within the region of strong tidal influence. The present study attempted to develop a practical methodology that would enable them to apply a commonly used numerical model, such as the 2D shallow-water equation model, to simply evaluate ocean tides that propagate upstream in an estuary under fluvial influences without specifying the upstream discharge.

2. Study Area and Data

The authors obtained water-level data for Dinh An, Can Tho, and Chau Doc in the Hau River, Vietnam (**Fig. 1**).

(1) Water level data of study area

The Mekong Delta begins in Phnom Penh, Cambodia, where the river divides into its two main distributaries, the Hau and the Tien, forming the delta in Vietnam with a vast triangular plain of about 55,000 km^2 (Mekong River Commission [MRC], 2005). Tides enter the Hau River through two river mouths, divided by a coastal sandbank, where Dinh An and many other small towns are located (**Fig. 1**). Then, tides reach Can Tho (situated about 80 km inland from the river mouth) in a few hours, continue to propagate further upstream to Chau Doc, near Cambodia's border (about 190 km inland), where it disappears (MRC, 2005; Thao *et al*., 2014; Esteban *et al*., 2015; Fujihara *et al*., 2015; Takagi *et al*., 2015, 2016b).

We obtained hourly WL data for the period between July 2009 and June 2010 (**Fig. 2a**; during this period no significant data are missing) at three locations, Dinh An, Can Tho, and Chau Doc, monitored by a Vietnamese governmental agency (the Southern Regional Hydro-Meteorological Centre). The completed one-year period data are considered sufficient for fundamental tidal analysis. Although these observatories are located in the same river of the Mekong Delta (Hau River), data should exhibit different characteristics of WLs depending on various factors such as river discharge, bottom friction, and geometry of the river.

The weather in Southern Vietnam is characterized by two monsoon seasons: the Southwest monsoon, which brings heavy rain, and the Northeast monsoon, which causes dry weather (Thao *et al*., 2014). The measured WLs at Chau Doc (190 km from the sea) shown in **Fig. 2a** also demonstrate the presence of two distinctive seasons,

ACCEPTED MANUSCRIPT

flood and dry seasons. The flood season is clearly identified by the sharp increase in maximum WL with no significant daily fluctuations, whereas WLs in the dry season show dynamic tidal fluctuations similar to those observed at the other two locations, Dinh An and Can Tho. Considering this annual trend in WLs in Chau Doc, we see that the peaks during the flood and dry seasons occur in two periods around October and April, respectively, as also corroborated by the other researches (*e.g.,* MRC, 2009). Thus, this classification is used in the following analyses.

(2) Water level after removing seasonal variations

Fig 2b shows the water changes associated with semi-diurnal tides (mainly composed of four tidal constituents: M2, S2, N2, and K2), which were extracted using a band-pass filter in order to see how predominant tidal oscillations will be transformed between these locations. **Fig. 2b** seems to exhibit that tidal amplification appears during the peak flood season (around September to October) at Dinh An, likely induced by high river discharge.

WLs at Dinh An are considered less influence by river discharge, while WLs at Chau Doc may be less influenced by tides, and predominantly determined by fluvial flow. The Hau River is an ideal candidate for this study because its nearly straight geometry makes the meandering effects on tidal damping less important. Likewise, another merit for focusing on this river is that standing waves, which result in a complicated flow regime, are not developed because the estuary does not have a strongly convergent shape. The estuary shape number is defined as the ratio of the square root of the river depth to the convergence length of the estuary, which is one of the main indicators for estuary characteristics. Savenije *et al*. (2008) demonstrated that the Hau River with a low estuary shape number and a high phase lag between high water and high water slack is subject to more tidal damping than ordinary estuaries.

ACCEPTED MANUSCRIPT

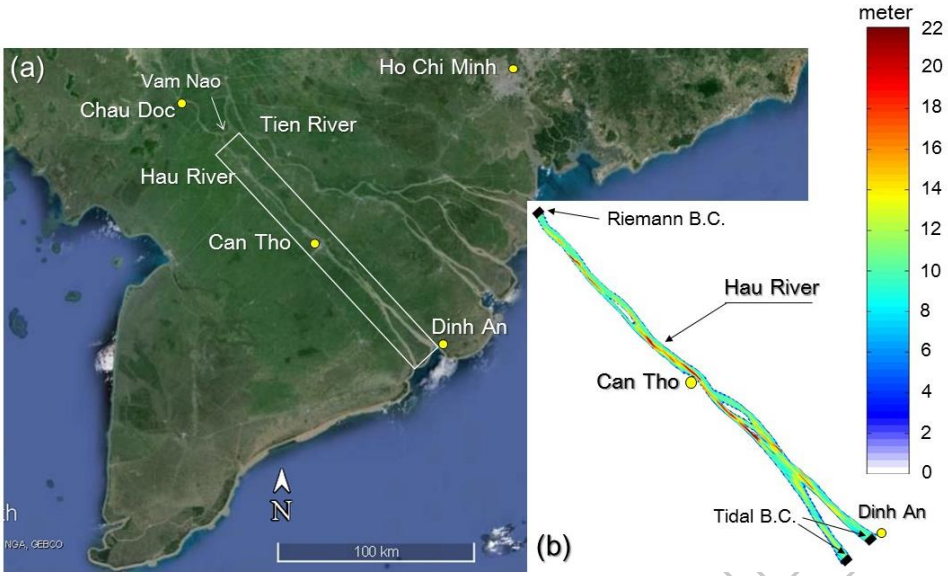

Fig. 1 (a) Map indicating three sites, Dinh An, Can Tho, and Chau Doc, in Hau River, where water level data were obtained. The thin rectangle indicates the extent of the computational domain, focusing particularly on Can Tho. **(b)** Boundary conditions (B.C.) assigned in the numerical model and bathymetry within the study area.

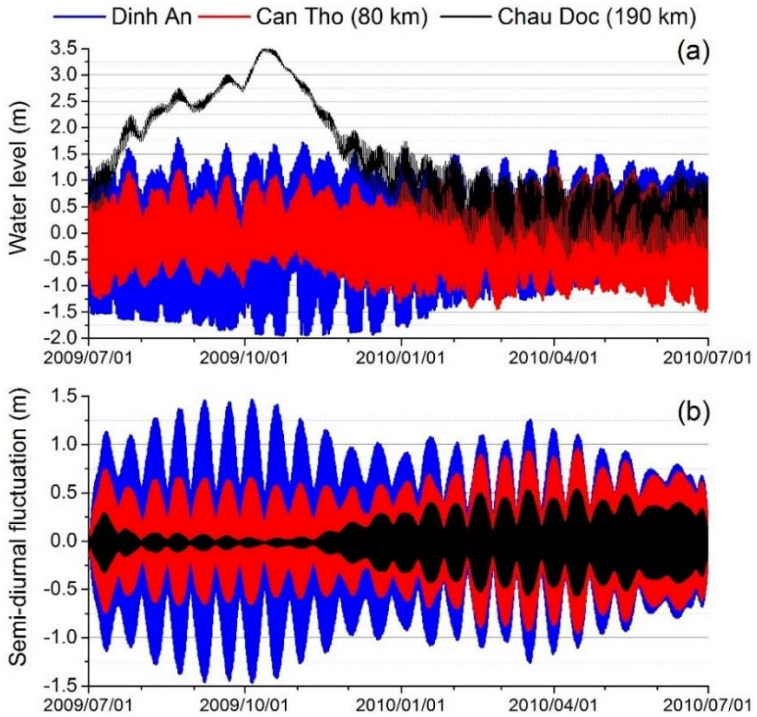

Fig. 2 Water levels (WL) at three locations in the Hau River. The peak flood season is considered to typically occur around October, and the dry season around April. **(a)** Original data; **(b)** semi-diurnal WL fluctuation (mainly composed of four tidal

constituents: M2, S2, N2, and K2), after removing seasonal variations.

3. Methodology

This section explains a series of analyses, including spectrum analysis and hydrodynamic simulations, to propose the practical tide model without imposing an upstream discharge boundary.

(1) Manning's *n* values

Amongst many parameters to be assigned, bed friction is one of the most fundamental settings to determine the accuracy of the numerical model. The Gauckler-Manning coefficient, often denoted by n (hereinafter referred to as Manning's n), is often used to represent friction in simulations performed by coastal engineers (e.g. Bricker *et al.*, 2015). This parameter is an empirical coefficient that depends on various factors such as surface roughness and sinuosity. For example, the n values for a flood plain were proposed by Arcement and Schneider (1984) as follows:

$$n = (n_b + n_1 + n_2 + n_3 + n_4)\, m \tag{1}$$

where n_b is a base value of n for bare soil surface, n_1 is a value reflecting the effect of irregularities on the flood plain, n_2 is a coefficient for variations in shape and size of the river cross section, n_3 is a coefficient for obstructions, n_4 is a value for vegetation on the flood plain, and m is a correction factor for the sinuosity of the flood plain.

(2) Procedures for numerical modelling

In this study an additional coefficient is added to **Eq. 1** in order to explicitly take into account energy loss caused by interactions between river discharge and incoming ocean tides. **Fig. 3** outlines the proposed procedure leading to the determination of an appropriate value of Manning's n, which is applicable to an ocean–river connecting model.

In the first step, Fourier analysis was applied to investigate the frequency characteristics of WLs at multiple locations in the studied estuary, namely Dinh An, Can Tho, and Chau Doc. The conventional FFT method (the Cooley-Turkey algorithm)

ACCEPTED MANUSCRIPT

was applied to analyse the data. This analysis enabled us to calculate the propagating ratio *r*, which is defined as the wave amplitude at a given location upstream divided by that near the river mouth (the damping ratio can be calculated as 1- *r*).

In the next step, a numerical simulation (shallow-water equation model for this study) imposing the predominant tidal wave, typically a semi-diurnal tide, was performed to seek the Manning's *n* value that can best fit the aforementioned propagating ratio. In this study, Manning's *n* was separately determined for a flood and dry seasons because it was expected that each season has distinctive tidal damping characteristics that are highly dependent on the river discharge rate. In southern Vietnam, the lunar M2 semi-diurnal constituent is greater than any others (see **Table A-1**); therefore, the step (d) in **Fig. 3** only investigated the influences of M2 tides, while the final step of (g) was performed for actual tides composed of many constituents in **Table A-1**.

Delft3D-FLOW (Deltares, 2011) was implemented for the simulation of tides that travel upstream from the river mouth to the estuary. The present study used a 2D horizontal grid, instead of a full 3D domain; thus, the code simplifies to a shallow water equation. Depth-averaged models are often used in engineering practice to simulate environmental flows in coastal and river regions (Cea *et al.*, 2007). The Delft model adopts the ADI (Alternating Direction Implicit) method for time integration, which splits one-time step into two stages (Deltares, 2011).

The computational domain encompassed a long stretch of the Hau River between 9.5°N–106.1°E and 10.6°S–105.4°E (**Fig. 1b**) with the smallest-size grid cells being 180 m (cross-sectional direction) × 1400 m (flow direction). The grid size in the cross-sectional direction was set to be particularly fine in order to sufficiently reproduce narrower streams divided by sandbanks. Time increment for the numerical computation is selected 12 sec. Can Tho is positioned in the middle of the domain (**Fig. 1b**), while Chau Doc is located outside the domain. For simplicity, we excluded an upstream part of the Hau River near Chau Doc because there is a major confluence connecting it to the Tien River (Vam Nao; **Fig. 1**), which requires a more complex treatment of the upstream boundary. Water depths, which have been investigated by multiple institutes and research groups (including the authors' group, e.g., Quan *et al.*, 2014) over the last several years and converted from Mean Sea Level (MSL) as a

ACCEPTED MANUSCRIPT

reference level, were used in the model (**Fig. 1b**).

The bathymetric data were relatively new and cover the long stretch of the Hau River. However, any engineering structures such as concrete dykes were not precisely reproduced. In addition, the channels of the Mekong Delta have displayed irregular and complex bed changes, including significant incision and expansion and deepening of numerous pools, accelerated by upstream development (e.g., dam construction; Brunier *et al*., 2014). Construction of dams will also alter the seasonal flow variability in the upper Mekong River (Le *et al.*, 2007). Although this study did not consider such possible transition of the river morphology in recent periods, it should be noted that all these factors would also have some influence on behaviour of tides propagating the estuary.

(3) Boundary conditions of numerical modelling

It appears that the treatment of the boundaries is more difficult for simulating the hydraulics in the flood season than that in the dry season in the case of the Mekong Delta. It would be better to extend the model beyond the limit of tidal influence and to specify the actual river discharge. The Southern Regional Hydro-Meteorological Centre of Vietnam measures river velocity with a current meter in Hau River. However, gross discharge rates are substantially influenced by tidal currents because all hydrological stations managed by this institute are being measured in the low land subject to tidal influence. Thus, the net downstream river discharge needs to be estimated by some other method. For example, the flow rate can be determined by repeating the simulation with a number of different river discharge rates in order to identify the condition which best reproduces the observed WLs at the observatory, as performed by Takagi *et al*. (2018). However, this procedure appears to pose a laborious task for engineers to specify the discharge because it changes with time and various conditions.

We proposes the simplified methodology without a river discharge upstream boundary, which is possible to simulate tidal propagation along the river only by imposing tidal constituents along the ocean-side boundary (**Fig. 1b**). The upstream boundary was kept as an open boundary (referred to as the Riemann Boundary, which enables progressive waves to pass through the boundary without reflection). The ocean

ACCEPTED MANUSCRIPT

tidal constituents were obtained by conducting harmonic analysis on the WL data from the observatory at Dinh An (**Table. A-1**), as these WLs should correspond to ocean tides. Because of the negligence of river discharge, the proposed method cannot reproduce the resultant WL combined by tides and discharge. However, the amplitudes of tides and their damping can be readily evaluated by adjusting Manning's *n* value, as discussed in the following section.

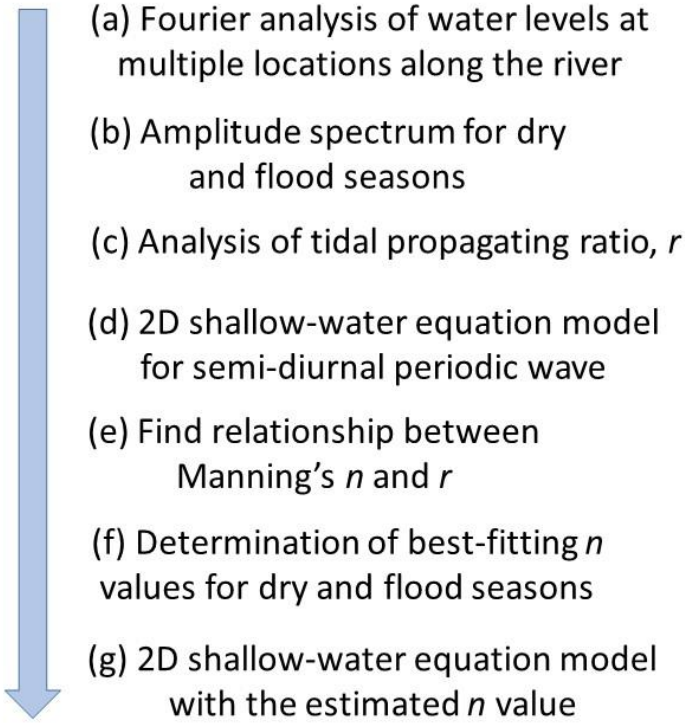

Fig. 3 Procedure to estimate Manning's *n* for use in shallow-water equation model connected to an estuary.

4. Results and Discussion

This section demonstrates that intensified tidal damping during flood season can be readily reproduced using the numerical model with a best-fit Manning's *n* value.

(1) Amplitude spectrum and propagating ratio

Fig. 4 shows the amplitude spectrum for three locations derived by the FFT method applied to three different intervals (the whole year, the dry season, and the flood season). The semi-diurnal component can be considered to govern water fluctuations, followed by the diurnal and annual components in both Dinh An and Can Tho. On the other hand, **Fig. 4 (c-1)** suggests that WLs are predominantly determined by seasonal variations (semi-annual and annual fluctuations) in the case of Chau Doc, demonstrating strong fluvial and pluvial influences. Nevertheless, there also exist two remarkable peaks around the semi-diurnal and diurnal periods shown in **(c-1)**, which clearly indicate the existence of oceanic influences. In the flood season, tides virtually disappear before they reach Chau Doc **(c-3)**, whereas tides can substantially propagate in the dry season **(c-2)** over a distance as long as 190 km.

Fig. 5 shows the tidal propagating ratio that is defined as the amplitude spectrum in Can Tho (or Chau Doc) divided by that in Dinh An. It is noted that we calculated the propagating ratio based only on the semi-diurnal fluctuation, since it appears to be predominant throughout the year in Can Tho (**Fig. 4**). The analysis results indicate that the propagating ratio is only 51% in the flood season (damping ratio of 49%), but 74% in the dry season (damping ratio of 26%). This suggests that tides are significantly attenuated in the flood season. Since the effect of river discharge is negligible in the dry season (Takagi *et al*., 2015), tidal damping of up to about 26% is likely caused by bottom friction. **Fig. 5** also shows that tides propagate farther, while attenuating at a constant rate, and almost disappear in the flood season before they reach Chau Doc. Again, it is noted that tides can easily propagate in the dry season, and about 42% of the wave amplitude of an incident tide still remains even in Chau Doc.

ACCEPTED MANUSCRIPT

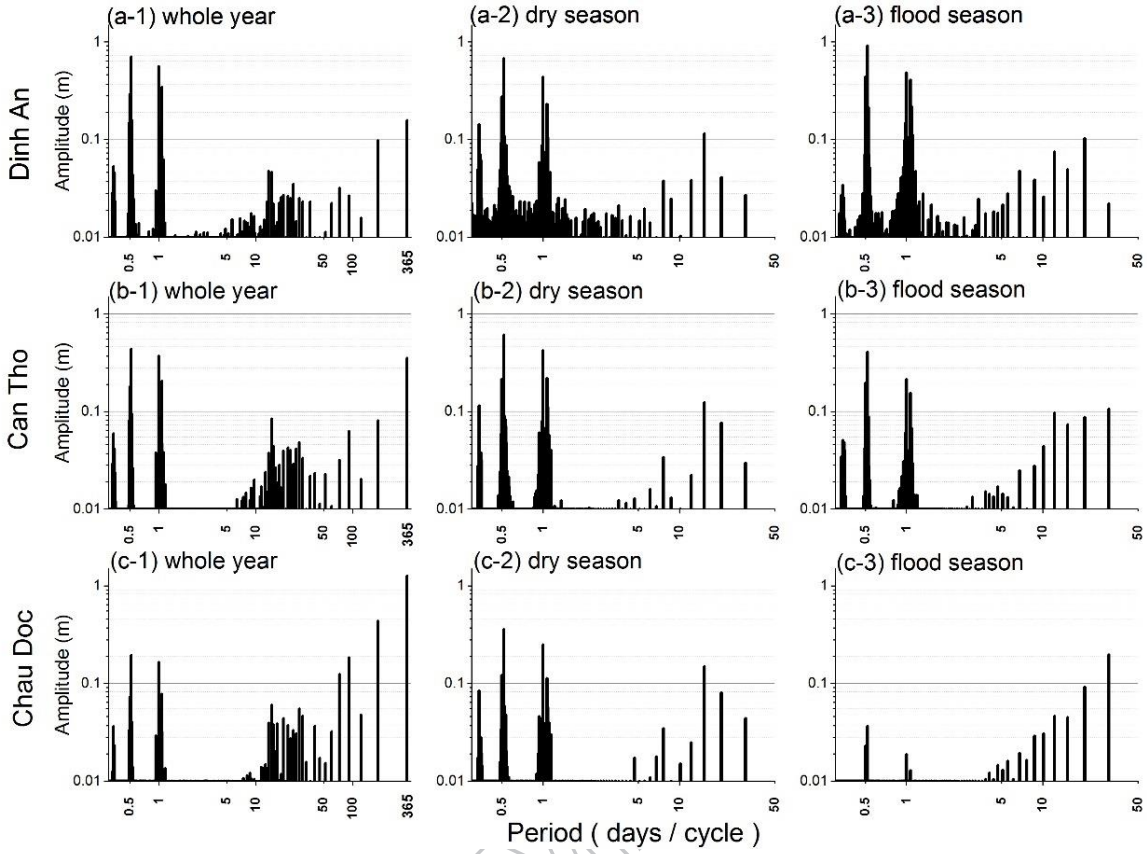

Fig. 4 Amplitude spectrum at Dinh An (river mouth), Can Tho (80 km inland), and Chau Doc (190 km inland) for three seasons: whole year (left), dry season (middle), and flood season (right). Data for the whole year cover short to long periods of waves (up to one year), while the analysis for dry and flood seasons reveal the frequency characteristics for periods of up to two months.

ACCEPTED MANUSCRIPT

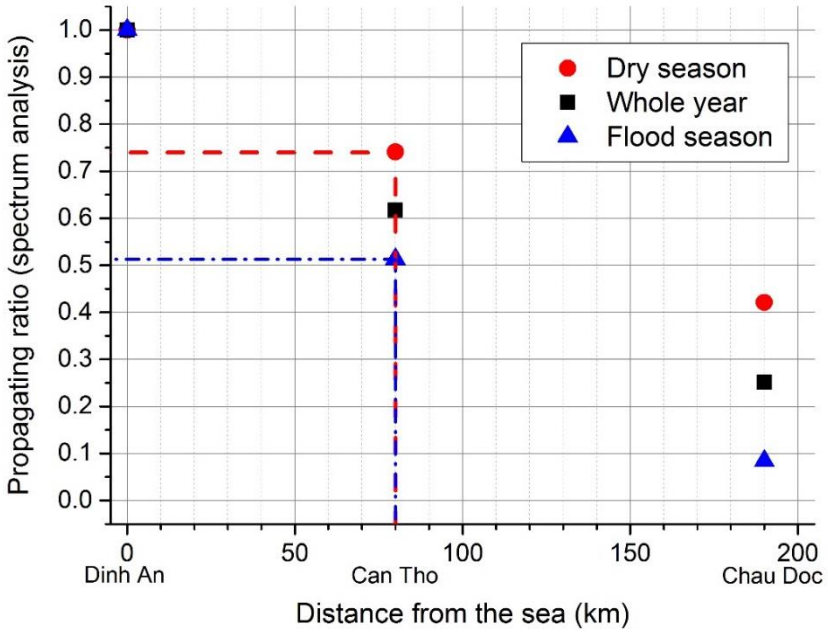

Fig. 5 Tidal propagating ratio obtained by comparing semi-diurnal amplitude spectrum between Can Tho (or Chau Doc) and Dinh An. The ratio lies in the range between 51% and 74% in the case of Can Tho, demonstrating significant variation depending on the season.

(2) Estimated Manning's *n* values by numerical simulation

Fig. 6 shows the relationship between Manning's *n* value and the tidal propagating ratio, *r*. The values of *r* are calculated by comparing tidal amplitudes at two locations, Dinh An and Can Tho, using the Delft3D-FLOW model imposing five different *n* values from 0.01 to 0.05. The *n* value can also be estimated using the asymptotic equation (**Fig. 6**):

$$n = 0.0028 + 0.1354\exp(-2.981r) \quad (2)$$

where *r* is the dimensionless tidal propagating ratio and *n* is Manning's *n* value with a dimension of [s $m^{-1/3}$]. The larger the propagating ratio, the smaller Manning's *n* value.

The propagating ratios in the flood season, dry season, and whole year are estimated to be approximately 0.51, 0.74, and 0.61 respectively, based on spectrum

ACCEPTED MANUSCRIPT

analysis of the observed data. Consequently, **Fig. 6** suggests that the Manning's *n* value that best reproduces tidal damping over the distance of 80 km from Dinh An to Can Tho is estimated to be *n* = 0.032, 0.018, 0.025 in the flood season, dry season, and whole year, respectively.

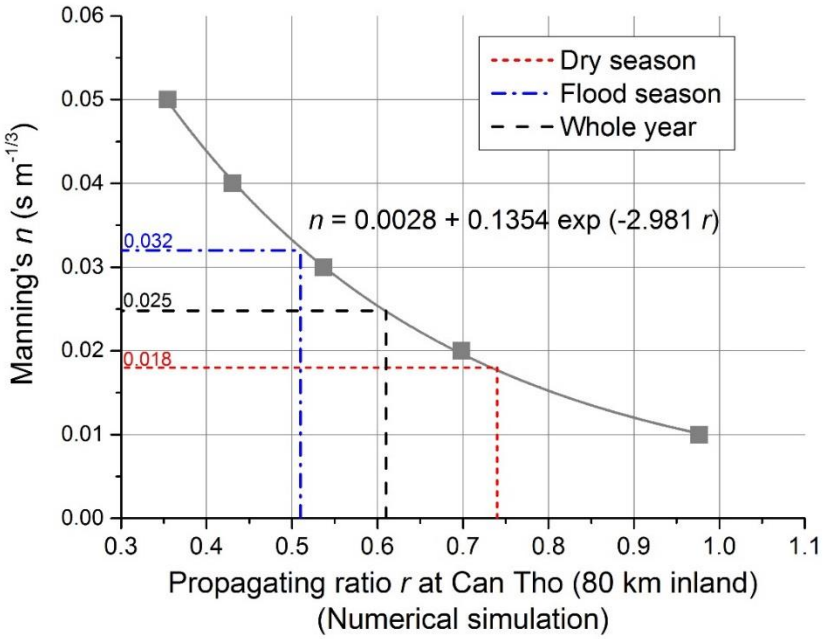

Fig. 6 Relationship between Manning's *n* and propagating ratio *r* (defined as the M2 amplitude in Can Tho divided by that in Dinh An), derived by a numerical simulation imposing a semi-diurnal periodic wave from the river mouth boundary (**Fig. 1b**). The red dashed-dotted line shows estimation of Manning's *n* for the dry season, while the blue dashed line corresponds to the flood season. The propagating ratios are derived from **Fig. 5**.

(3) Proposed Manning's *n* values

Note that both **Fig. 5** and **Fig**. **6** were obtained by considering only the component of semi-diurnal WL fluctuations, as these were considered to be predominant among all the frequencies. The estimated Manning's *n* values, 0.032 and 0.018 for the flood and dry seasons, respectively, are thus valid only for a flow regime composed of semi-diurnal tides. However, actual tides are composed of multiple waves of different amplitudes, frequencies, and phase lags, naturally making prediction more difficult.

Fig. 7 shows a comparison between observed and simulated WLs in Can Tho

ACCEPTED MANUSCRIPT

during a four-day period in the flood and dry seasons. The simulation was performed by imposing eight tidal constituents as shown in **Table A-1**. October was considered a typical month in the flood season, while April was typical of the dry season as mentioned earlier. In the flood season, the simulated WL with Manning's n values as high as 0.025–0.032 showed reasonable agreement with the observations, while the simulation with n = 0.018 seemed to result in a slight overestimation of tidal amplitude by a few tens of cm. On the other hand, it appears that the simulation with n = 0.018 provides the best estimation among three options in the dry season, demonstrating less tidal damping influence.

Arcement and Schneider (1984) indicated that n values for straight uniform channels composed of sand range from 0.012 to 0.026. Similarly, Simons (1985) presents values of 0.012 to 0.022 for the plane bed. The estimated value for the dry season in the Mekong Delta lies within these ranges, whereas the maximum n value for the flood season is out of this range. However, the values in the flood season (0.025–0.032) are similar with those presented by Demissie and Bacopoulos (2017), in which they surveyed the lower St. Johns River in June 2009 and estimated Manning's n values in the estuary being 0.029 and 0.022 for ebb and flood tide, respectively.

Fig. 8 provides a more comprehensive analysis to evaluate which Manning's n value should be assumed to reproduce tidal damping using a longer period of data. The amplitude spectrum was calculated using the analysis for **(a)** April as a typical dry season month and **(b)** October as a typical flood season month. These figures compare the amplitude of observed and simulated WLs by decomposing the data into component waves with different frequencies based on Fourier analysis, as mentioned earlier. The simulation using n = 0.032 appears to underestimate WLs during the dry season (**Fig. 8 (a)**), while n = 0.018 results in a slight overestimation during the flood season (**Fig. 8 (b)**). These differences in best-fitting n values suggest the importance of using an appropriate value of n, which inevitably changes according to the season.

Considering the best-fitting Manning's n varies with the season, **Eq. 1** can be reformulated by incorporating a new parameter as follows:

$$n = (n_b + n_1 + n_2 + n_3 + n_4 + n_5)\ m \tag{3}$$

ACCEPTED MANUSCRIPT

where n_5 is a newly introduced parameter associated with tidal damping due to river discharge. Note that n_5 is compensation for the proposed simplification that discharge is not specified at the upstream boundary. This study suggests that the resultant n can be assumed to be 0.018 for the dry season and 0.025–0.032 for the flood season.

Parameter m in **Eq. 3** can be taken as unity, since the Hau River runs almost in a straight line, as explained earlier. The sum of the parameters from n_b through n_4 can thus be assumed to be 0.018 because the tidal damping effect due to river discharge is almost negligible during a typical dry season, resulting in a value of zero for n_5. Assuming that parameters other than n_5 can be kept constant in flood seasons, it is expected that a flood condition will contribute to increase the value of n by 0.007–0.014 relative to the dry season n value, interpreted as a significant flow resistance increase of 39%–78%.

Among these parameters in **Eq.3**, however, the vegetation-relevant factor n_4 appears to vary in a spatial and temporal manner because the presence of vegetation, especially in the floodplain, affects the overall friction (e.g., seasonal growth of macrophytes). Therefore, it is recommended that friction coefficients can be specified based on the growth of aquatic plants (Morin *et al*., 2000, Matte *et al*., 2017b, Takagi 2018). For the case of the Mekong Delta, however, the seasonal vegetation area may not substantially change because tropical forest covers the floodplain throughout the year. Bottom friction may also not be significantly influenced by seasonal changes in inundated areas because WLs in the delta are not remarkably different between flood and dry seasons, typically within a few tens of centimetres, because of low-lying nature of the land (Takagi *et al*., 2018). Although more detailed analysis is required to prove this hypothesis, the variability associated with seasonal vegetation growth could be indirectly compensated by the proposed Manning's n which considered seasonal changes in river discharge

ACCEPTED MANUSCRIPT

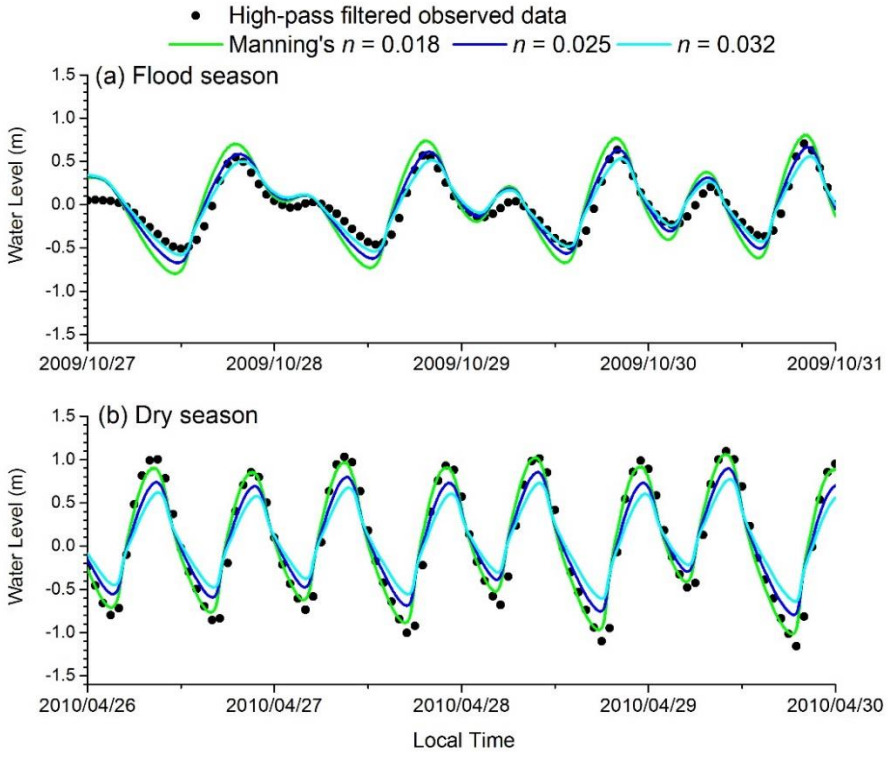

Fig. 7 Observed and simulated water levels (WLs) in Can Tho during **(a)** flood season and **(b)** dry season. A high-pass filter was applied to remove seasonal WL trends from the original observed data, which enables direct comparison of observed WLs with those simulated by the numerical model.

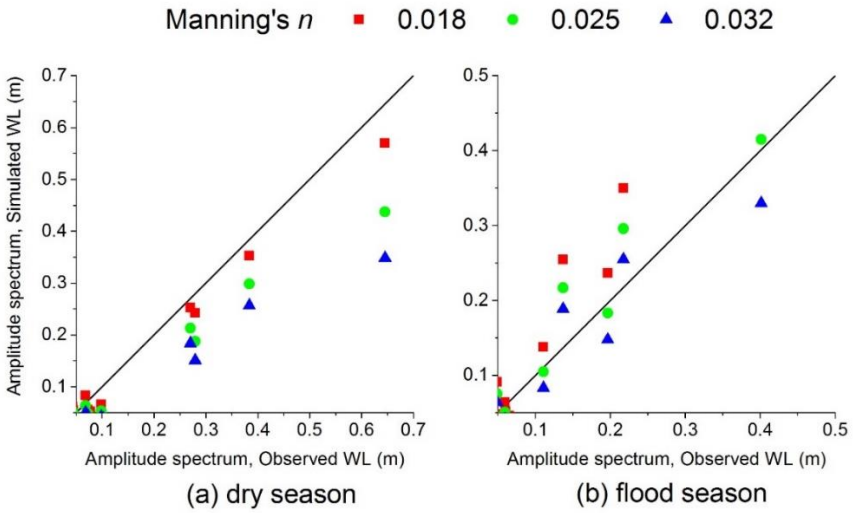

Fig. 8 Comparison of amplitude spectra derived from observed and simulated water levels (WLs) in Can Tho, using data for **(a)** the dry season (April 2010) and **(b)** the flood season (October 2009).

(4) Flow velocities

The authors also obtained flow velocity data for the station in the midstream of the Hau River in Can Tho, where the water depth is about 15 m, which is operated by the Hydrological Center in the Cuu Long River. These data were compared with those simulated with Delft3D Flow (**Fig. 9**). The periods correspond with the flood and dry seasons in the same way as those in **Fig. 7**. The flow velocities were measured every hour with current meters deployed at six different vertical positions in the water. The depth-averaged velocities were derived by averaging the vertical velocities.

As shown in **Fig. 9a**, the observed velocities mostly show positive values in the flood season, demonstrating the existence of strong river flows against tidal flows. As mentioned earlier, river discharge was not taken into account and the Riemann Boundary was assigned as the upstream boundary instead. Therefore, the simulation cannot correctly reproduce the mean velocity (or residual velocity) especially when river discharge is high. However, in order to directly compare between observed and simulated velocities in the flood season, those lines derived with the simulation were purposely shifted upward by 0.75 m/s to fit with the mean value of the observed velocity. On the other hand, the observed velocities in the dry season show more or less symmetrical patterns into both the positive and negative values, demonstrating that the effect of river discharge is negligible. Hence, the simulated results in the dry season did not require modification, in contrast to the flood season.

The selection of Manning's *n* value appears to affect the magnitude of velocities. The best-fit *n* value seems to lie in between 0.025 and 0.032 in the case of the flood season, whereas *n* of between 0.018 and 0.025 can well predict velocities during the dry season. In this way, the present study demonstrated that changes in Manning's *n* value according to river flow conditions result in more reliable estimations of flow velocities as well as WLs than simply using a constant value throughout the year.

ACCEPTED MANUSCRIPT

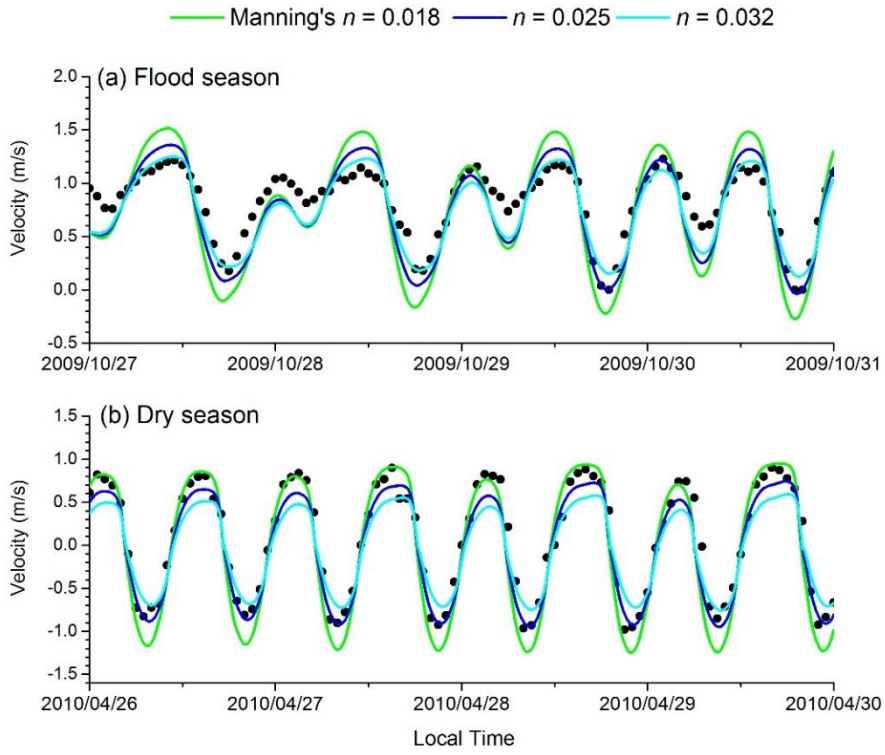

Fig. 9 Observed and simulated depth-averaged velocities in Can Tho during **(a)** flood season and **(b)** dry season. Positive values of velocity indicate flow directions towards the sea, while negative values indicate landward flows.

(5) Discussion

The proposed *n* values will be of great benefit particularly for practicing engineers because they can evaluate river WLs, which are largely influenced by ocean tides, without imposing an upstream river discharge boundary. Nevertheless, the authors acknowledge that the proposed methodology is still in its infancy because it neglects some important characteristics affecting hydraulics in estuarine environment. For example, the shallow-water equation model used in the present study did not consider the detailed physical interaction between fresh river water and seawater, which may alter hydraulics in the estuarine environment. Vertical and horizontal shear in tidal currents generate fine-scale turbulence. The overall rate of mixing in estuaries could be determined by a combination of small-scale turbulent diffusion and a larger scale variation of the advective velocity field (Fischer *et al*., 1974; Prandle, 2009). Estuary stratification could be developed by the density difference between seawater and fresh

ACCEPTED MANUSCRIPT

river water.

The boat survey that measured vertical salinity distribution in dry season at several points in Hau River confirmed that a strong salinity (ca. 25 ppt) was observed at the river mouth, but it rapidly decreased by 1 ppt at about 50 km from the sea during a high-tide phase (Nguyen and Savenije, 2006). Therefore, in general salt wedge does not reach Can Tho city, which is about 80 km from the river mouth. The plot with the observed data (**Fig. 10**) shows that velocity profiles tend to follow a logarithmic curve, which does not demonstrate any noticeable stratification caused by salt wedge. The velocity data were measured with an on-board current meter, which is situated in the midstream of Hau River (**Fig. 11**). Hayes (1975) also classified the Vietnamese Mekong as a meso-tidal estuary where river water is mostly or partially mixed with seawater. Therefore, the authors consider that seawater and freshwater interactions do not significantly have to do with the phenomenon of tidal damping in the Mekong Delta as they are well mixed in the estuary. However, if the estuarine is defined as highly stratified with a fully developed salt wedge, the depth-averaged velocity approximation could be invalid as upper and lower water bodies would move in the opposite direction.

As clarified in the previous sub-section, observed and simulated velocities in the flood season were directly compared by adjusting those averaged values to each other, as shown in **Fig 9 (a)**. However, **Fig 10 (a)** shows all the raw data that essentially direct towards downstream side. This fact demonstrates that in flood season mass of river water moves towards the sea as a whole, while tides still convey substantial energy and propagate towards the upstream side as a form of wave. This strong counter flow in flood season should promote tidal damping and retard the speed of tidal propagation.

ACCEPTED MANUSCRIPT

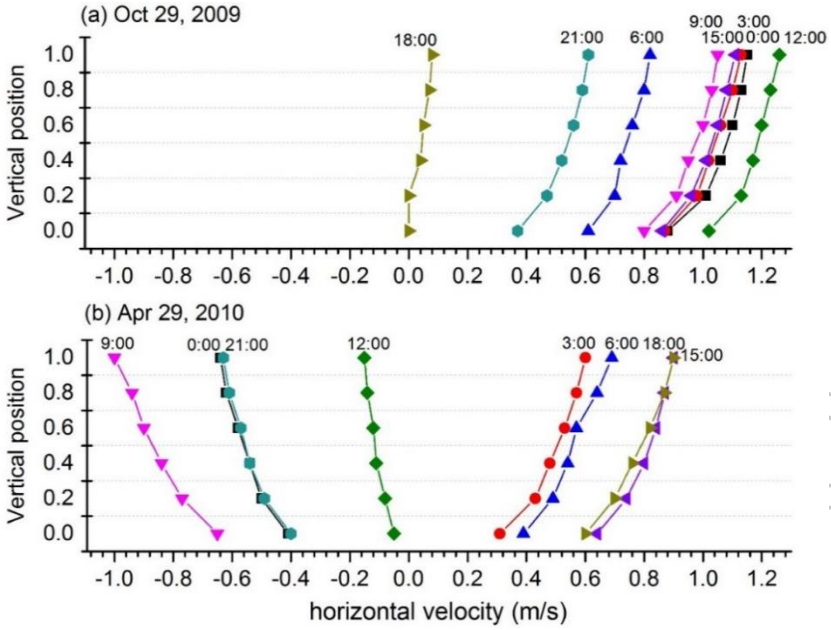

Fig. 10 Measured horizontal velocities at six vertical positions in the midstream of Hau River, Can Tho, on (a) 29 October 2009 (flood season) and (b) 29 April 2010 (dry season). Positive values indicate a flow direction towards the sea, while negative values indicate flows towards the upstream side.

Fig. 11 Velocity measurement on an anchored boat in the midstream of Hau River, operated by the Hydrological Center in the Cuu Long River, the Southern Regional Hydro-Meteorological Centre (near Can Tho City, Location: 10°02’51.3’’N, 105°48’00.0’’E)

ACCEPTED MANUSCRIPT

5. Conclusions

This study proposed the simplified modelling of ocean tidal propagation in the Mekong Delta that can be performed with seasonally varying Manning's *n* values instead of imposing an upstream discharge boundary. Modellers need to estimate a realistic range of *n* values to fit the stream of interest. The amplitude spectrum for three locations derived by the FFT method played an important role to find out a best-fitted *n* value for different seasons. For the stretch from the river mouth to Can Tho, tidal damping in the numerical model has an *n* value of 0.018–0.025 in the dry season and 0.025–0.032 in the flood season. It is recognized that flood-season conditions will significantly increase flow resistance by 39%–78%. The procedure and methodologies proposed in this study are expected to enable engineers/scientists to readily evaluate the influences of tidal damping in simulating ocean tides in estuaries. The model, which seamlessly connects the sea to the river without specifying the upstream discharge, will be of great benefit not only for tidal modelling but also river and urban flood simulations, saline intrusion modelling, typhoon storm surge and tsunami predictions, and future SLR projections.

Acknowledgements

This research was funded by the JSPS KAKENHI Grant Number 26702009 and 16KK0121 (Japan Society for the Promotion of Science). The authors thank, Tran Van Ty and Vinh Giap Vanat, for their valuable assistance in accomplishing this study.

References

Arcement, G.J., Jr., Schneider, V.R. (1984) Guide for Selecting Manning's Roughness Coefficients for Natural Channels and Flood Plains. Report No. FHWA-TS-84-204, Federal Highway Administration.

Bricker J.D., Gibson S., Takagi H., Imamura F. (2015) On the need for larger Manning's roughness coefficients in depth-integrated tsunami inundation models. Coast. Eng. J. 57 (02), 13 p., doi: 10.1142/S0578563415500059

Brunier G., Anthony E. J., Goichot M., Provansal M., Dussouillez P. (2014) Recent morphological changes in the Mekong and Bassac river channels, Mekong Delta:

ACCEPTED MANUSCRIPT

The marked impact of river-bed mining and implications for delta destabilisation, Geomorphology 224, pp. 177–191.

Cea L., Puertas J., Vázquez-Cendón M. (2007) Depth Averaged Modelling of Turbulent Shallow Water Flow with Wet-Dry Fronts, Archives of Computational Methods in Engineering, 14(3), pp.303–341

Chang CH. et al. (2019) A model-aided satellite-altimetry-based flood forecasting system for the Mekong River, Environmental Modelling & Software, 112, 112-127.

Dang T. D., Cochrane T. A., Arias M. E., Tri P. D. V. (2016) Hydrological alterations from water infrastructure development in the Mekong floodplains, Hydrological Processes, 30(21), pp.3824-3838.

Dasgupta, S., Laplante B, Meisner C., Wheeler D., Yan J. (2007) The Impact of Sea Level Rise on Developing Countries: A Comparative Analysis, World Bank Policy Research Working Paper 4136.

Deltares (2011) Delft3D-FLOW – Simulation of multi-dimensional hydrodynamic flows and transport phenomena, including sediments, User Manual Delft3D-FLOW, The Netherlands, 690 pp.

Erban, L. E., Gorelick S. M., Zebker H. A. (2014) Groundwater extraction, land subsidence, and sea-level rise in the Mekong Delta, Vietnam. Environmental Research Letters, 9(8), 6p.

Esteban M., Takagi H., Shibayama T. (2015) Handbook of Coastal Disaster Mitigation for Engineers and Planners, Elsevier, 780 pp., ISBN: 978-0-12-801060-0

Esteban M., Jamero M. L., Nurse L., Yamamoto L., Takagi H., Thao N. D., Mikami T., Kench P., Onuki M., Nellas A., Crichton R., Valenzuela V. P., Chadwick C., Avelino J., Tan N., Shibayama T., Adaptation to sea level rise on low coral islands: Lessons from recent events, Ocean & Coastal Management, 168, 35-40, 2019.

Fischer H.B., List E.J., Koh R.C.Y., Imberger J., Brooks N.H. (1979) Mixing in inland and coastal waters. Academic Press, New York, 483 pp.

Fujihara Y., Hoshikawa K., Fujii H., Kotera A., Nagano T., Yokoyama S. (2016) Analysis and attribution of trends in water levels in the Vietnamese Mekong Delta.

ACCEPTED MANUSCRIPT

Hydrol. Process, Vol. 30 (6), pp. 835–845, doi: 10.1002/hyp.10642.

Godin G. (1999) The propagation of tides up rivers with special considerations on the Upper Saint Lawrence River, Estuarine, Coastal and Shelf Science, 48, 307–324

Hayes M. O. (1975) Morphology of sand accumulation in estuaries. IN: Cornin L. E. (ed), Estuarine Research, Vol. 2, Academic Press, New York, pp. 3-12.

Hoang L. P., Lauri H., Kummu M., Koponen J., van Vliet M.T.H., Supit I., Leemans R., Kabat P., Ludwig F. (2016) Mekong River flow and hydrological extremes under climate change, Hydrol. Earth Syst. Sci., 20, 3027–3041.

IPCC (2013) Working Group I Contribution to The IPCC Fifth Assessment Report Climate Change 2013: The Physical Science Basis, Final Draft Underlying Scientific-Technical Assessment, 2216 pp.

Le T. V. H., Nguyen H. N., Wolanski, E., Tran T. C., Haruyama S. (2007) The combined impact on the flooding in Vietnam's Mekong River delta of local man-made structures, sea level rise, and dams upstream in the river catchment, Estuarine, Coastal and Shelf Science, 71, 110–116.

Matte P., Secretan Y., Morin J. (2017a) Hydrodynamic Modeling of the St. Lawrence Fluvial Estuary. II: Reproduction of Spatial and Temporal Patterns

Matte P., Secretan Y., Morin J. (2017b) Hydrodynamic modeling of the St. Lawrence fluvial estuary. I. Model setup, calibration and validation, Journal of Waterway, Port, Coastal, and Ocean Engineering, 143(5), 15p.

Mekong River Commission (MRC) (2005) Overview of the Hydrology of the Mekong Basin. ISSN: 1728 3248.

Mekong River Commission (MRC) (2009) The flow of the Mekong, MRC Management Information booklet series No. 2, 11 pp.

Morin J., Leclerc M., Secretan Y., Boudreau P. (2000) Integrated two-dimensional macrophytes-hydrodynamic modeling, Journal of Hydraulic Research, 38, 163-172.

Nguyen A. D., Savenije H.H.G. (2006), Salt intrusion in multi-channel estuaries: a case study in the Mekong Delta, Vietnam, Hydrol. Earth Syst. Sci., 10, 743–754.

Nhan N.H. (2016) Tidal regime deformation by sea level rise along the coast of the

ACCEPTED MANUSCRIPT

Mekong Delta, Estuarine, Coastal and Shelf Science, doi: 10.1016/j.ecss.2016.07.004

Prandle D. (2009) Estuaries –Dynamics, Mixing, Sedimentation and Morphology, Cambridge University Press, UK, 236p.

Quan N. H., Hieu N. Q., Nhan N. H., Dien L. D. (2014) Water quality modeling for assessing wastewater receiving capacity in lower Mekong Rivers. The 2nd International Conference on Computational Science and Engineering (ICCSE-2014) August 21st- 23rd, 2014, Ho Chi Minh City, Vietnam.

Sasaki J., Ito K., Suzuki T., Wiyono U. A., Oda Y., Takayama Y., Yokota K., Furuta A., Takagi H. (2012) Behavior of the 2011 Tohoku Earthquake Tsunami and resultant damage in Tokyo Bay, Coastal Engineering Journal, Vol.54, 26p.

Savenije H.H.G. (2001) A simple analytical expression to describe tidal damping or amplification, Journal of Hydrology, 243, 205–215.

Savenije H.H.G., Toffolon M., Haas J., Veling E.J.M. (2008) Analytical description of tidal dynamics in convergent estuaries, Journal of Geophysical Research, 113, C10025, 18 p., doi: 10.1029/2007JC004408

Simons L. (1985) Design manual for engineering analysis of fluvial systems, Arizona Department of Water Resources, Project Number AZ-DWR-05, 292p.

Takagi H., Tran T.Y., Thao N.D. (2014a) Investigation on floods in Can Tho City: influence of ocean tides and sea level rise for the Mekong Delta's largest city, In Coastal Disasters and Climate Change in Vietnam: Engineering and Planning Perspectives, Thao N.D., Takagi H., Esteban M. (eds.), Elsevier, New York, U.S., 257–274. doi: 10.1016/B978-0-12-800007-6.00012-5.

Takagi H., Bricker J. (2014b) Assessment of the effectiveness of general breakwaters in reducing tsunami inundation in Ishinomaki, Coastal Engineering Journal, Vol. 56, No. 4, 21p., doi: 10.1142/S0578563414500181.

Takagi H., Ty, T.V., Thao, N.D., Esteban, M. (2015) Ocean tides and the influence of sea-level rise on floods in urban areas of the Mekong Delta. Journal of Flood Risk Management, 8: 292–300. doi: 10.1111/jfr3.12094.

Takagi H., Thao N.D., Anh L.T. (2016a) Sea-Level Rise and Land Subsidence: Impacts

ACCEPTED MANUSCRIPT

on Flood Projections for the Mekong Delta's Largest City, Sustainability, 8(9), 959; doi:10.3390/su8090959.

Takagi H., Tsurudome C., Thao N.D., Le T.A., Tran V. T., Van P.D.T. (2016b) Ocean tidal modelling for urban flood risk assessment in the Mekong Delta, Hydrological Research Letters, Vol. 10, No. 1, pp. 21–26, doi: 10.3178/hrl.10.21.

Takagi H., Esteban M., Mikami T., Fujii D. (2016c) Projection of coastal floods in 2050 Jakarta, Urban Climate, doi: 10.1016/j.uclim.2016.05.003.

Takagi H., Tri V. P. D., Ty T. V., Thao N. D., Anh L. T., Vinh G. V. (2016d) Flow Intensification Induced by Tidal Oscillations in Tributaries of The Mekong River, International Journal of Safety and Security Engineering, Vol. 6 (3), pp. 697-703.

Takagi H., Anh T T, Anh L T, Thao N D, Takabatake T, Nakamura R. (2018) Mechanisms of Rapid Flow caused by Tidal–Fluvial Flow Interaction in Inland Waterways of the Mekong Delta IOP Conference Series: Earth and Environmental Science, 8 p.

Takagi H. (2018) Long-Term Design of Mangrove Landfills as an Effective Tide Attenuator under Relative Sea-Level Rise. Sustainability, 10, 1045.

Tasnim K.M., Shibayama T., Esteban M., Takagi H., Ohira K., Nakamura R. (2014) Field observation and numerical simulation of past and future storm surges in the Bay of Bengal: case study of cyclone Nargis, Natural Hazards, doi: 10.1007/s11069-014-1387-x.

Thao N.D., Takagi H., Esteban M. (Ed.) (2014) Coastal Disasters and Climate Change in Vietnam -Engineering and Planning Perspectives, Elsevier, 424 pp., ISBN: 978-0128000076.

Thuy H. P. T., Furukawa M. (2007) Impact of sea level rise on coastal zone of Vietnam. Bulletin of the College of Science, University of Ryukyu, 84, 45–59.

Tran Anh, D.; Hoang, L.P.; Bui, M.D.; Rutschmann, P. Simulating Future Flows and Salinity Intrusion Using Combined One- and Two-Dimensional Hydrodynamic Modelling—The Case of Hau River, Vietnamese Mekong Delta. Water 2018, 10, 897.

Vongvisessomjai S., Srivihok P. (2003) The interaction between tide and salinity

ACCEPTED MANUSCRIPT

barriers, Journal of Science and Technology, 25(6), 743–756.

Wassmann, R., Hien, N.X., Hoanh, C.T. and Tuong, T.P. (2004) Sea Level Rise Affecting the Vietnamese Mekong Delta: Water Elevation in the Flood Season and Implications for Rice Production. Climatic Change 66, 89-107.

Appendix

Table A-1 Eight principal tidal constituents at Dinh An Station: Amplitude and phase

Tidal constituent	Amplitude (m)	Phase (deg)
M2	0.885	210.5
S2	0.323	250.1
N2	0.180	190.6
K2	0.111	253.7
K1	0.616	221.5
O1	0.442	177.9
P1	0.192	220.2
Q1	0.079	175.4

ACCEPTED MANUSCRIPT